scientific reports

Check for updates

OPEN

Discrepancies in precipitation changes over the Southwest River Basin of China based on ISIMIP3b

Yunkai Zhang[1], Juan Du[1]✉, Yibo Ding[1,2], Lingling Wu[3] & Tianqi Ao[1,4]✉

Selecting appropriate global climate models (GCMs) is crucial for minimizing uncertainty in regional climate projections under future scenarios. Previous studies have predominantly assessed the modeling capability of GCMs for regional precipitation climatology and its long-term patterns based on annual and seasonal precipitation data. Building upon these, we primally evaluated the performance of five GCMs from phase 3b of the Inter-Sectoral Impact Model Intercomparison Project (ISIMIP3b) in simulating precipitation concentration and its variations in the Southwest River Basin (SWRB) of China using the precipitation concentration index (PCI). The results indicate that: (1) The 5 GCMs generally capture the spatial distribution of annual average precipitation in the SWRB but significantly overestimate its magnitude, with a maximum regional average deviation of 207.80 mm. Furthermore, all models tend to overestimate the overall drying trend in the SWRB and show limited capability in simulating interdecadal variations of annual precipitation. (2) While the 5 GCMs reasonably simulate the spatial distribution of annual average PCI in the SWRB, they tend to overestimate its values, with a maximum regional average deviation of 1.54. Additionally, their simulation performance in capturing PCI trends and interdecadal variations is also limited. (3) The 5 GCMs tend to overestimate seasonal precipitation in the SWRB, with the best simulation performance for the distribution of autumn precipitation, followed by spring and summer, and the poorest for winter. Significant differences exist in the simulation performance of the models for seasonal precipitation proportions, which result in discrepancies in the models' representation of PCI. Moreover, the models' poor simulation performance of PCI trends is partly due to their inadequate modeling of trends in seasonal precipitation proportions. The findings will contribute to laying the foundation for meteorological hydrological research and water resource management in the SWRB.

Keywords ISIMIP3b, Comparative assessment, The Southwest River Basin, Precipitation changes, Precipitation concentration index

Global warming directly affects precipitation patterns, accelerating surface evaporation and increasing atmospheric water vapor content, leading to more frequent occurrence of extreme hydrological events worldwide, significantly impacting human activities, livelihoods, and biological ecosystems[1]. Projected temperature changes over the next 20 years suggest that global warming is expected to reach or exceed 1.5 °C, indicating that continued global warming is essentially inevitable without intervention[2,3]. Therefore, it is necessary to study the characteristics of precipitation pattern changes in different regions and to make predictions about future precipitation changes to deepen our understanding of the evolution of the climate system and to provide a scientific basis for water resources management and disaster prevention under climate change. The Southwest River Basin (SWRB), located in southwestern China, is characterized by complex topography and significant elevation differences. Influenced by climate systems such as the East Asian Monsoon and the South Asian Monsoon, this region exhibits longitudinal, latitudinal, and vertical climatic variations. In the context of global warming, the SWRB has experienced a significant increase in severe precipitation events[4,5], impacting both its socio-economic development and natural ecological systems. Therefore, it is essential to accurately predict future precipitation changes in the SWRB.

[1]State Key Laboratory of Hydraulics and Mountain River Engineering, College of Water Resource & Hydropower, Sichuan University, No. 24 South Section 1, Yihuan Road, Chengdu 610065, China. [2]Yellow River Engineering Consulting Co., Ltd, Zhengzhou 450003, China. [3]Sichuan Hydrological and Water Resources Survey Center, Chengdu 611130, China. [4]Institute for Disaster Management and Reconstruction, Sichuan University-Hong Kong Polytechnic University, Chengdu 610065, China. ✉email: dujuan@stu.scu.edu.cn; aotianqi@scu.edu.cn

Global climate models (GCMs) are fundamental for understanding and forecasting climate and its changes, providing estimates of future climate change based on various emission scenarios. Currently, they are widely used in climate simulation, prediction, and risk assessment[6,7]. To effectively address the challenges of climate change, the World Climate Research Programme (WCRP) Working Group on Coupled Modelling (WGCM) has organized a series of Coupled Model Intercomparison Projects (CMIPs) to support global climate simulation and projections[8]. The Inter-Sectoral Impact Model Intercomparison Project (ISIMIP), jointly initiated by the Potsdam Institute for Climate Impact Research (PIK) in Germany and the International Institute for Applied Systems Analysis (IIASA), has generated various model datasets with different emission scenarios based on the CMIP's GCMs data. These datasets aim to enhance the understanding of global and regional climate change impacts, improve risk characterization across different sectors, and provide policymakers with relevant information[9]. At present, ISIMIP has advanced to its third phase (ISIMIP3), which includes the release of the ISIMIP3a and 3b protocols in February 2020. For the GCMs provided by CMIP, ISIMIP not only standardizes them to a grid resolution of 0.5°×0.5° but also proposes a statistical bias correction method premised on maintaining long-term trends of meteorological elements. This method corrects historical datasets by applying a constant temperature offset or multiplicative correction factor for precipitation, regardless of the time scale[10,11]. Due to these advantages, the ISIMIP has been extensively utilized in climate change impact studies across various regions. However, significant uncertainties surround the direct use of GCMs for regional climate change projections, primarily due to model uncertainty, internal climate system variability, and scenario uncertainty. Of these, model uncertainty is deemed the most influential[12]. Moreover, since the large number of available GCMs and their varying performance across different regions of the world[13], indicating that an objective assessment of their suitability in the region of interest should be conducted before the formal utilization of GCMs.

Recently, numerous scholars have assessed the performance of GCMs in various regions using diverse criteria. Zhou et al.[14] used spatial correlation coefficients, simulation deviation, and root-mean-square errors to preliminarily evaluate the basic performance of four Chinese models in CMIP6, and discovered that the ensemble mean of these models reproduced the spatial distribution of global temperature and precipitation well. Jia et al.[15] utilized an improved rank score method to evaluate the performance of 33 GCMs from CMIP5 in simulating precipitation over the Tibetan Plateau, and the results indicated that while most GCMs reasonably simulated the annual precipitation cycle and the temporal characteristics of precipitation, they exhibited shortcomings in reproducing its spatial distributions. Fiedler et al.[16] assessed the performance of CMIP6 models in simulating tropical precipitation using various indicators and compared them with the earlier generations of GCMs. The assessment showed that the GCMs from the CMIP6 performed better than the CMIP3 and CMIP5 in terms of tropical mean spatial correlations and the root-mean-square error of the climatology of tropical precipitation.

Previous studies primarily assessed the performance of GCMs in simulating the spatial and temporal distribution of precipitation and its variation characteristics in various regions based on annual and seasonal values. While these variables partly reflect the basic climatic state and long-term patterns of precipitation, they have limitations in describing temporal irregularity of precipitation. However, the temporal distribution of precipitation throughout the year is crucial because it can indicate changes in the hydrological cycle and the risk of extreme precipitation events, and provide guidance for land use planning[17,18]. To analyze the monthly concentration of annual precipitation, Oliver[19] proposed a monthly Precipitation Concentration Index (PCI), which was later developed by De Luis et al.[20]. This index, based on monthly precipitation data, quantitatively evaluates the heterogeneity of monthly precipitation throughout the year and effectively represents the concentration and seasonality of precipitation[19,20]. Compared to other indicators of precipitation concentration, the PCI stands out for its simplicity in calculation and clear physical meaning, making it a popular choice in studies concerning spatiotemporal patterns of precipitation changes[21–23]. Unfortunately, few studies have evaluated the simulation performance of GCMs for PCI and its trend. Therefore, in response, this study evaluates the ability of five GCMs from the ISIMIP3b to simulate the PCI and its trend in the SWRB from 1961 to 2014 and analyzes the reasons for the simulation differences among the models.

Therefore, this study comprehensively evaluates the performance of five ISIMIP3b models for the characteristics of precipitation changes in the SWRB from 1961 to 2014, based on annual and seasonal precipitation and PCI values. The objectives are as follows: (1) to assess the simulation performance of the five GCMs for the spatiotemporal patterns and variations of annual precipitation in the SWRB; (2) to evaluate the representation of the five GCMs for the monthly precipitation concentration and its variations in the SWRB using PCI; (3) to assess the abilities of the five GCMs to simulate the spatiotemporal patterns and variations of seasonal precipitation in the SWRB, and to analyze the reasons for differences in their PCI simulation capabilities. Results from our study will contribute to mitigating the adverse effects of future climate change for government departments and water resource management agencies and provide a basis for the sustainable development of water resources in the SWRB.

Data and methods

Study area

The SWRB is a region located in southwestern China, between 21°–35°N and 77°–106°E (Fig. S1), covering an area of approximately 850,000 km². It is part of the Tibetan Plateau and Yunnan-Guizhou Plateau. The SWRB is characterized by numerous high mountains, plateaus, and canyons, exhibiting steep terrain and diverse topography, encompassing various climate types. It boasts the highest average altitude and greatest altitude difference in China. Additionally, the SWRB is rich in water resources, being traversed by two major international rivers, the Yarlung Zangbo River and the Lancang River. However, the social-economic development and water resource utilization in the SWRB lag behind other regions of China due to its complex terrain and varying natural conditions. Furthermore, the SWRB exhibits a trend of frequent extreme precipitation events against the backdrop of global warming. Due to its distinctive geographical location, there is a pressing need for research

on the impacts of climate change in the SWRB. This research is crucial for effectively addressing the challenges posed by climate change and providing data support for water resource protection.

Observation data and ISIMIP3b models

A gridded observational dataset (CN05.1) produced by China Meteorological Administration is used to evaluate the models. CN05.1 is generated by interpolating data collected from 2416 meteorological stations across China with a spatial resolution of 0.25°[24]. Up to now, the dataset is still continuously being updated. For ease of comparison, we selected the CN05.1 daily precipitation data from 1961 to 2014 in the SWRB, and interpolated it to the same 0.5° grid as the ISIMIP3b models by using bilinear interpolation method.

The model data used in this study are historical simulation experiment datasets from ISIMIP3b, which selected five CMIP6 models based on the responses of Global Impact Models (GIMs) to CMIP climate change projections. These datasets include 5 models and 11 meteorological variables from CMIP6, all uniformly interpolated to a 0.5°×0.5° latitude-longitude grid. According to the research of Jägermeyr et al.[25], the five GCMs selected by ISIMIP3b are structurally independent with respect to their ocean and atmosphere model components, and they collectively represent the range of equilibrium climate sensitivity (ECS) within the entire CMIP6 ensemble. Furthermore, the mean and standard deviation of ECS and transient climate response (TCR) for these five GCMs perfectly match those of the full 38-member CMIP6 ensemble. For this study, we selected global daily precipitation data from these five models (GFDL-ESM4, IPSL-CM6A-LR, MPI-ESM1-2-HR, MRI-ESM2-0, and UKESM1-0-LL) for the period 1961–2014. Only the first realization (usually r1i1p1f1, except r1i1p1f2 for UKESM1-0-LL) of each model was used. Basic information about the models is provided in Table S1, with further details available on the ISIMIP official website (https://www.isimip.org/).

In this study, the seasons are defined as follows: spring from March to May, summer from June to August, autumn from September to November, and winter from December to February of the following year. The observed and simulated precipitation for each season is calculated by summing the precipitation amounts for the corresponding months using the CN05.1 and ISIMIP3b datasets, respectively.

Methods

Precipitation concentration index

In this study, we characterized the concentration degree and seasonality of annual precipitation in the SWRB using the precipitation concentration index (PCI). This index enabled us to evaluate the simulation performance of five ISIMIP3b models regarding the precipitation concentration and its variations in the SWRB. The PCI calculation method we employed was proposed by De Luis et al.[20], which was an improvement on the definition introduced by Oliver[19]. PCI is defined as follows:

$$PCI = \frac{\sum_{i=1}^{12} p_i^2}{\left(\sum_{i=1}^{12} p_i\right)^2} \times 100 \tag{1}$$

where p_i represents the precipitation amount for the ith month. According to Eq. (1), if the total annual precipitation is concentrated in one month, the PCI is 100, reaching its maximum value. Conversely, if the total annual precipitation is evenly distributed over 12 months, the PCI achieves its minimum value, approximately 8.33. In practical applications, internationally recognized definitions are used: PCI < 10 indicates a uniform monthly distribution of annual precipitation; 10 < PCI < 15 indicates a relatively uniform monthly distribution; 15 < PCI < 20 indicates an uneven monthly distribution with seasonal variations; and PCI > 20 indicates an exceptionally concentrated distribution with significant monthly variations.

From Eq. (1), the PCI value for a given year can be obtained by using the monthly precipitation data for that year. The multi-year average PCI calculated in this study is the arithmetic mean of the PCI values for each year within the selected period, while the regional average PCI is the average of all grid point PCI values in the spatial domain.

Taylor diagram and Taylor skill score

The Taylor diagram, initially proposed by Taylor[26], serves as a fundamental tool for assessing the performance of different models by comparing the similarity and differences between model simulations and observations. It relies on three key metrics: spatial correlation coefficient, centered normalized root-mean-square error, and spatial standard deviation ratio of the modeled and observed values[26]. These three metrics can be represented on a polar plot, where the radial distance from the origin to a specific point indicates the spatial standard deviation of the model field relative to the observed field, and the azimuthal position corresponds to the spatial correlation coefficient between the two fields. The distance between the specific point and the reference point (REF) represents the centered normalized root-mean-square error of the model field. In this study, the Taylor diagram was used to visually depict the spatial modeling capacities of five ISIMIP3b models for historical precipitation changes in the SWRB. The more skillful the ISIMIP3b models are in reproducing the spatial variation of observational data, the closer both the spatial correlation coefficient and the ratio of spatial standard deviation are to 1, and the closer the normalized root-mean-square error is to 0. Considering the subjectivity in assessing the spatial modeling capacities of ISIMIP3b models only by Taylor diagram, the Taylor skill (TS) scores of the models were further calculated to quantitatively reflect the relative performance of model simulations, as proposed by Taylor[26]. TS is defined as follows:

$$\mathrm{TS} = \frac{4 \times (1+R)^4}{\left(\frac{\sigma_m}{\sigma_o} + \frac{\sigma_o}{\sigma_m}\right)^2 \times (1+R_0)^4} \tag{2}$$

where R represents the spatial correlation coefficient between observation and model fields, R_0 is the maximum value of R among the selected models, σ_m and σ_o are the standard deviations of the model and observed values, respectively. The TS value ranges from 0 to 1, with higher values indicating better spatial modeling capacity of the model as compared to other models.

Interannual variability skill score

To quantitatively assess the ISIMIP3b models' capacities to reproduce the temporal variations of observational data, we introduced the interannual variability skill (IVS) score. This score evaluates the models' capacity to simulate the interannual variability of the time series at each grid point[27,28]. IVS is defined as follows:

$$IVS = \left(\frac{STD_m}{STD_o} - \frac{STD_o}{STD_m}\right)^2 \tag{3}$$

where STD_m and STD_o represent the interannual standard deviations of the model and observed values, respectively. We first calculated the IVS for each grid point in space and then computed the regional average to obtain the IVS scores for different variables. This calculation method can offer a more rigorous assessment of models compared with other calculation methods, such as calculating interannual standard deviations using area mean values and then calculating the IVS. When STD_m equals STD_o, the IVS value is 0. A lower IVS value indicates a better capacity of the model to reproduce the interannual variability.

Results

Performance analysis of annual precipitation

Figure 1 illustrates the spatial distribution of the multi-year average precipitation in the SWRB from 1961 to 2014, as simulated by five ISIMIP3b models and observations. The observed annual average precipitation in the SWRB generally decreases from southeast to northwest. In the northern part, it is mostly less than 500 mm, while in the central part it ranges from 500 to 1000 mm, and in the southern part it is roughly between 1000 and 2000 mm. Although the five models generally capture the gradient distribution of annual average precipitation, they still exhibit deficiencies in terms of quantity and certain details. Specifically, all models tend to overestimate

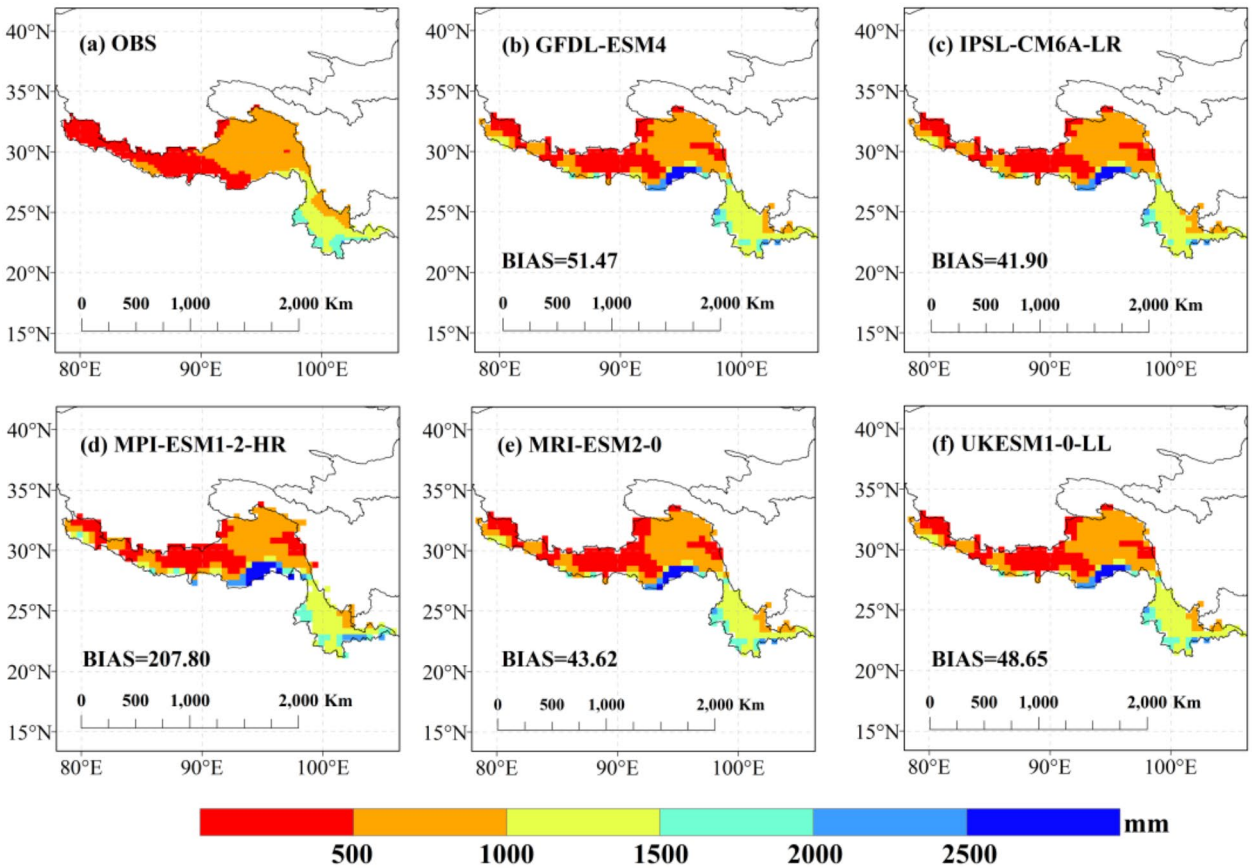

Fig. 1. The spatial distribution of climatology for annual precipitation in the SWRB from 1961 to 2014 (unit: mm): (**a**) CN05.1 observation; (**b**–**f**) 5 ISIMIP3b models. "BIAS" represents the average deviation of each model (unit: mm).

annual precipitation across the entire SWRB. The MPI-ESM1-2-HR model exhibits the largest average deviation among the models, reaching 207.80 mm, while the IPSL-CM6A-LR model shows the smallest deviation, with an average of 41.90 mm. The remaining three models have average deviations of no more than 52.00 mm. Notably, the overestimation of all models is most significant in the marginal regions. Furthermore, similar to most GCMs simulating precipitation over the western plateau of China, the five ISIMIP3b models also simulate a false precipitation peak in the Himalayan region. This is likely due to the insufficient resolution of current GCMs, making it challenging to accurately represent the steep terrain and complex underlying surface conditions in the Himalayan region.

The results shown in the Taylor diagram (Fig. S2) indicate that, except for the MPI-ESM1-2-HR model, the other four models exhibit relatively good spatial simulation performance for annual average precipitation in the SWRB, with spatial correlation coefficients mainly between 0.65 and 0.70. Moreover, the standard deviation ratio between simulated and observed precipitation exceeds 1.00 for all models, with four models around 1.50 and the MPI-ESM1-2-HR model nearing 2.00. This indicates that all models generally overestimate the spatial variability of annual precipitation in the SWRB. Furthermore, the standardized root-mean-square errors for all models are greater than 1.00, with the MPI-ESM1-2-HR model exceeding 1.50. These findings collectively indicate that the spatial modeling capacities of all models for annual average precipitation in the SWRB remain somewhat constrained.

The model's spatial and temporal modeling capacities for the climatological annual precipitation in the SWRB are quantified by using the Taylor skill (TS) score and the interannual variability skill (IVS) score, respectively. Thus, we derive a comprehensive ranking of the five models' performance in simulating the climatological annual precipitation in the SWRB by aggregating rankings associated with each evaluation metric, as depicted in Table 1. Analysis of the TS values reveals that, except for the MPI-ESM1-2-HR model, the remaining four models generally yield TS values close to or exceeding 0.80. The UKESM1-0-LL model achieves the highest TS value (0.853), indicating its superior spatial modeling ability in capturing the climatological annual precipitation patterns within the SWRB. Furthermore, the assessment based on IVS values identifies the IPSL-CM6A-LR model as having the most proficient temporal modeling capability, with an IVS value of 1.111. From the comprehensive ranks, the IPSL-CM6A-LR model exhibits the best performance in characterizing the climatology and interannual variability of annual precipitation in the SWRB for the period 1961–2014.

The trend in precipitation variation, as another significant meteorological feature, serves as a crucial metric for assessing model simulation performance. Figure S3 illustrates the spatial distribution of annual precipitation trend in the SWRB during the period from 1961 to 2014, as simulated by five ISIMIP3b models and observed data. According to Fig. S3, the central and the Himalayan regions of the SWRB exhibit an overall trend towards wetter conditions, while the northern and southern regions show a trend towards aridity, with the southern region experiencing particularly intense dryness. The entire SWRB exhibits a drying trend, with a trend coefficient of − 0.08 mm/a. Regarding the arid conditions in the northern region, except for the IPSL-CM6A-LR and UKESM1-0-LL models, the remaining three models demonstrate relatively good simulation performance. For the overall wet conditions in the central region, the MPI-ESM1-2-HR model tends to overestimate, while the other four models tend to underestimate. In the southern region, the GFDL-ESM4, MPI-ESM1-2-HR, and UKESM1-0-LL models exhibit overestimation, with the GFDL-ESM4 model showing severe overestimation, while the IPSL-CM6A-LR and MRI-ESM2-0 models exhibit underestimation. For the regional average precipitation trend, all models overestimate the overall aridity trend in the SWRB, the MRI-ESM2-0 model simulates an average precipitation trend of − 0.17 mm/a, which is closest to the observed value. In contrast, the GFDL-ESM4 model deviates the most from the observation, with a simulated value of − 1.63 mm/a.

The Taylor diagram (Fig. S4) of the five ISIMIP3b models, regarding their capability to simulate the precipitation trend in the SWRB, demonstrates considerable room for improvement in spatial modeling capabilities concerning precipitation trend compared to their climate mean state. The spatial correlation coefficients vary among the models, with the MPI-ESM1-2-HR model showing the highest coefficient (0.72) with observed precipitation trend, followed by the GFDL-ESM4 and UKESM1-0-LL models at around 0.60, and the IPSL-CM6A-LR and MRI-ESM2-0 models ranging broadly from 0.40 to 0.50. Regarding the ratios of standard deviation, the ratios exceed 1.00 for all model fields, with values ranging from 1.00 to 1.50 for the IPSL-CM6A-LR and MRI-ESM2-0 models, and exceeding 1.50 for the other three models. All models exhibit standardized root-mean-square errors exceeding 1.00, with the IPSL-CM6A-LR model showing relatively smaller values.

To offer a more comprehensive illustration of each model's capacity to simulate the average precipitation trend within the SWRB, Fig. 2 delineates the temporal series of observed and simulated annual precipitation averages

Model	TS		IVS		Comprehensive rank
	Value	Rank	Value	Rank	
GFDL-ESM4	0.803	3	1.303	3	3
IPSL-CM6A-LR	0.806	2	1.111	1	1
MPI-ESM1-2-HR	0.395	5	4.254	5	5
MRI-ESM2-0	0.796	4	1.233	2	3
UKESM1-0-LL	0.853	1	1.340	4	2

Table 1. Ranks of 5 ISIMIP3b models about annual average precipitation over the SWRB according to their comprehensive performance considering both the TS and IVS values.

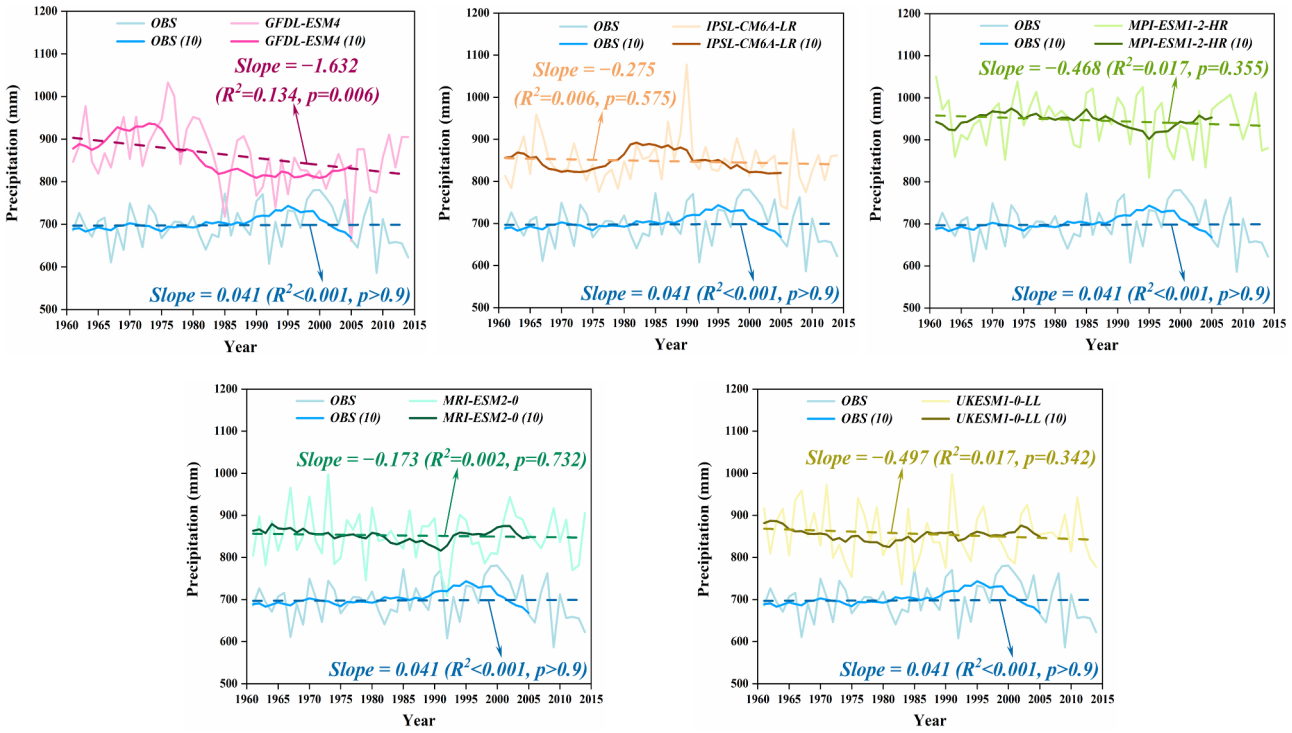

Fig. 2. The time series of observed and modeled annual precipitation in the SWRB from 1961 to 2014. "(10)" denotes a 10-year moving average applied to each precipitation series, and the dashed lines represent the linear trend lines of the original precipitation series.

over the SWRB spanning the years 1961 to 2014. Additionally, a 10-year moving average is applied to the annual precipitation series for each model to assess their ability to capture interdecadal variations in precipitation within the SWRB. The findings show that observed annual precipitation in the SWRB during the mentioned period exhibits a non-significant increasing trend, averaging 0.041 mm/a. Conversely, all models depict a declining trend in annual precipitation, with the GFDL-ESM4 model showing the most significant trend at − 1.632 mm/a. Furthermore, regarding the interdecadal fluctuations in precipitation within the SWRB, from the early 1960s to the late 1980s, the observed interannual fluctuations in precipitation exhibit small variability. Notably, only the GFDL-ESM4 and IPSL-CM6A-LR models fail to capture this characteristic. Of these, the GFDL-ESM4 model shows the most significant fluctuations, followed by the IPSL-CM6A-LR model. From the early 1990s to the early 21st century, the observed precipitation trends in the SWRB display fluctuations, transitioning from initial increases to subsequent decreases, ultimately manifesting as a declining trend in the early 21st century. Of the five models, only the MRI-ESM2-0 model simulates this feature, albeit with some temporal lag.

Overall, the simulation performance of the five models in representing the spatial distribution of annual precipitation trend in the SWRB from 1961 to 2014 is inadequate. However, when considering the TS value (Table omitted here) as a metric, the MPI-ESM1-2-HR model exhibits relatively superior performance, boasting a TS value of 0.676, while the MRI-ESM2-0 model records the lowest value (0.446), indicative of comparatively poorer simulation quality. Regarding the temporal variability of annual precipitation in the SWRB over the same period, none of the five models manages to accurately replicate the region's average trend. Nonetheless, the MPI-ESM1-2-HR, MRI-ESM2-0, and UKESM1-0-LL models demonstrate relatively commendable performance in capturing interdecadal precipitation variations from the early 1960s to the late 1980s. Furthermore, the MRI-ESM2-0 model exhibits relatively considerable proficiency in simulating interdecadal precipitation shifts from the early 1990s to the onset of the current century.

Performance analysis of precipitation concentration

Figure 3 illustrates the spatial distribution of multi-year average PCI in the SWRB from 1961 to 2014, as simulated by five ISIMIP3b models alongside observed data. The analysis reveals that during this period, a portion of the SWRB region exhibits PCI values ranging from 10 to 15, indicating a relatively uniform monthly precipitation distribution. In most areas, primarily concentrated in the central basin, the PCI ranges from 15 to 20, suggesting seasonal precipitation patterns with some degree of intra-annual concentration. Conversely, regions east of 80°E and south of 30°N show PCI values exceeding 20, signifying non-uniform precipitation distribution with notable variations in monthly precipitation amounts. Overall, the five models effectively capture these spatial features, with simulated PCI average deviations all below 2.00. Among them, the MPI-ESM1-2-HR model exhibits the smallest average deviation of 0.46, while the MRI-ESM2-0 model shows the largest, at 1.54. Furthermore, akin to the simulation of annual average precipitation, all models exhibit varying degrees of overestimation in certain areas of PCI. Notably, overestimations are evident in regions south of 30°N and near 100°E longitude for all

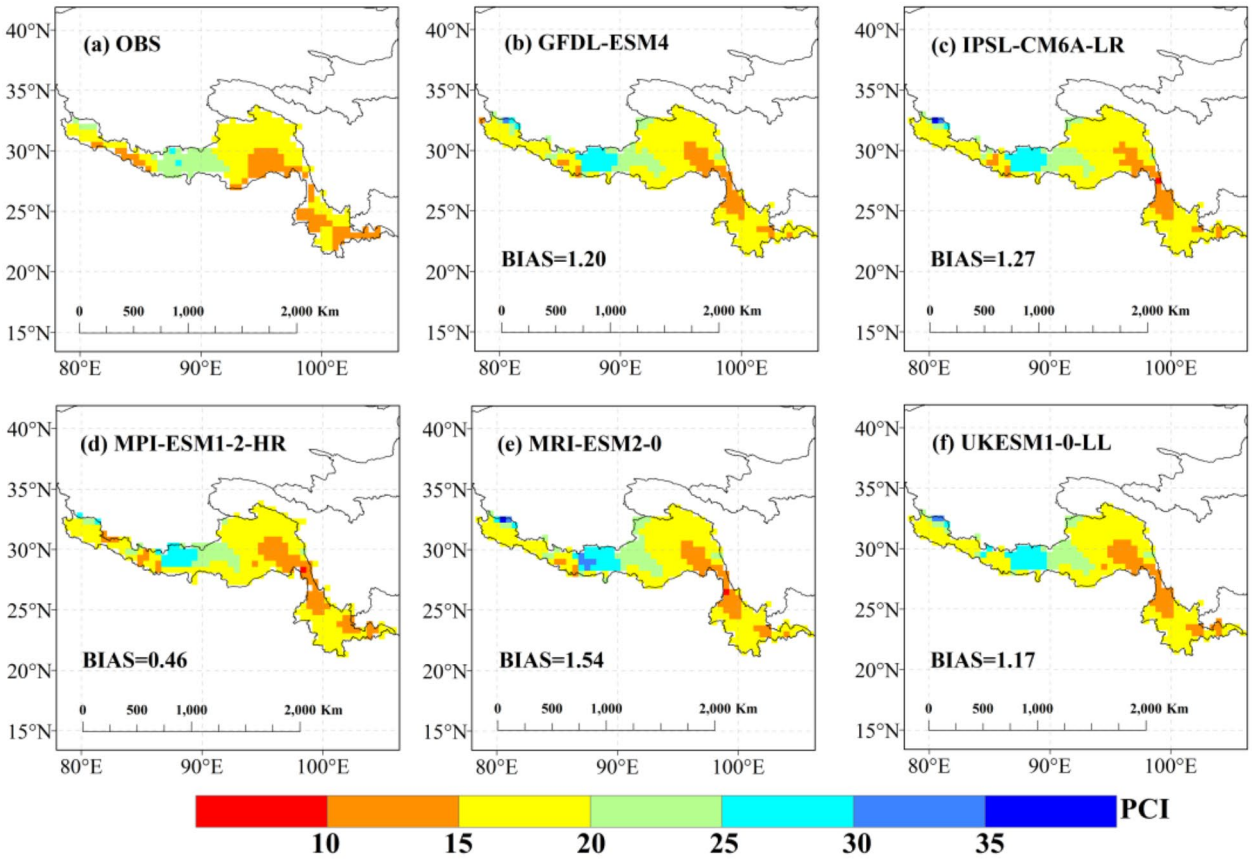

Fig. 3. The same as Fig. 1, but for the annual average PCI.

Model	TS		IVS		Comprehensive rank
	Value	Rank	Value	Rank	
GFDL-ESM4	0.763	2	1.188	3	2
IPSL-CM6A-LR	0.711	4	1.976	5	4
MPI-ESM1-2-HR	0.972	1	0.826	1	1
MRI-ESM2-0	0.678	5	1.668	4	4
UKESM1-0-LL	0.739	3	1.074	2	2

Table 2. The same as Table 1, but for the annual average PCI.

models. Additionally, the four models, apart from the MPI-ESM1-2-HR model, significantly overestimate PCI in the region east of 80°E. Moreover, regarding the false high precipitation center in the Himalayan region, all five models display a certain degree of overestimation in terms of PCI.

Quantitative results depicted in the Taylor diagram (Fig. S5) underscore the satisfactory simulation performance of all models for the annual average PCI in the SWRB. Spatial correlation coefficients between observation and model fields consistently surpass 0.80, with the MPI-ESM1-2-HR model notably exceeding 0.95. Furthermore, the ratios of standard deviation for all models generally range from 1.00 to 1.50, while the standardized root-mean-square errors are all less than 1.00. These findings suggest that the five models exhibit excellent performance in simulating the spatial distribution pattern of annual average PCI in the SWRB.

In a manner analogous to Table 1, Table 2 provides a comprehensive ranking of the simulation performance of the five models for the annual average PCI in the SWRB. At the spatial scale, the MPI-ESM1-2-HR model significantly outperforms the other models, boasting a TS value of 0.972. Similarly, on the temporal scale, the MPI-ESM1-2-HR model demonstrates superior simulation performance, with an IVS value of 0.826. Thus, the MPI-ESM1-2-HR model emerges as the optimal choice for simulating the annual average PCI in the SWRB from 1961 to 2014, owing to its superior spatial and temporal modeling capabilities.

The spatial distribution of trend coefficients for the PCI derived from observations and simulations by five ISIMIP3b models during the period 1961–2014 in the SWRB is illustrated in Fig. S6. Analysis indicates an overall decreasing trend in the PCI across the SWRB during the study period, with a regional average PCI trend coefficient of $-0.16(10\,a)^{-1}$, suggesting a trend towards a more uniform distribution of precipitation throughout the year. However, the simulation performance of the PCI trend coefficients by all models is generally inadequate. Specifically, for the southern region of the basin, only the GFDL-ESM4 and IPSL-CM6A-LR models exhibit relatively superior simulation results, while for the northern and central regions, the performance varies among the models, generally showing slightly better simulations for the northern region. In terms of regional average, only the MRI-ESM2-0 model simulates an average PCI trend closest to the observed value, at −0.07. Conversely, the MPI-ESM1-2-HR model shows the greatest deviation from the observed value, simulating a trend coefficient of 0.17.

Analysis of the corresponding Taylor diagram (Fig. S7) indicates that the spatial modeling capabilities of the five models for PCI trend coefficients are significantly lower than those for annual average PCI. The spatial correlation coefficients between model and observation fields range only from 0.10 to 0.40, with the UKESM1-0-LL model field showing the highest spatial correlation coefficient at 0.366. Furthermore, the standard deviation ratios for all models exceed 1.00, with the value for the MRI-ESM2-0 model approaching 2.00. Additionally, the standardized root-mean-square errors for all models exceed 1.00, with four models (except for the MPI-ESM1-2-HR model) surpassing 1.50. These findings suggest poor simulation performance of the spatial distribution pattern of annual PCI trend coefficients in the SWRB by all models. Based on the TS values, the simulation performance of the UKESM1-0-LL model is relatively optimal, with a TS value of 0.771.

Figure 4 presents the temporal series and interdecadal variations of observed and simulated PCI for the regional average in the SWRB from 1961 to 2014. Overall, all models generally overestimate the intra-annual concentration of precipitation in the SWRB, a trend that became particularly prominent since the 1990s. Moreover, regarding the regional average PCI trend coefficients, the MRI-ESM2-0 model exhibits the smallest simulation deviation, while the MPI-ESM1-2-HR model displays the largest deviation. Furthermore, similar to annual average precipitation, PCI in the SWRB also exhibits significant interdecadal variations. From the early 1960s to the 1970s, the PCI in the SWRB exhibited a decreasing trend, followed by successive fluctuating changes characterized by increases and decreases from the late 1970s to the early 21st century, with relatively small amplitude variations. Overall, the GFDL-ESM4 model relatively well simulates the interdecadal variations of PCI from the early 1970s to the mid-1990s, while the IPSL-CM6A-LR model exhibits a certain degree of temporal advancement in its simulation results during this period. However, neither of these two models captures the interdecadal variations of PCI in the SWRB during the early 1960s and the early 21st century, and the simulation performance of the other three models for the interdecadal variations of PCI is generally poor.

Performance analysis of seasonal precipitation

PCI effectively characterizes the irregularity and seasonality of annual precipitation. The variation of seasonal precipitation serves as a critical indicator of seasonal hydrological extremes, agricultural productivity, and habitat

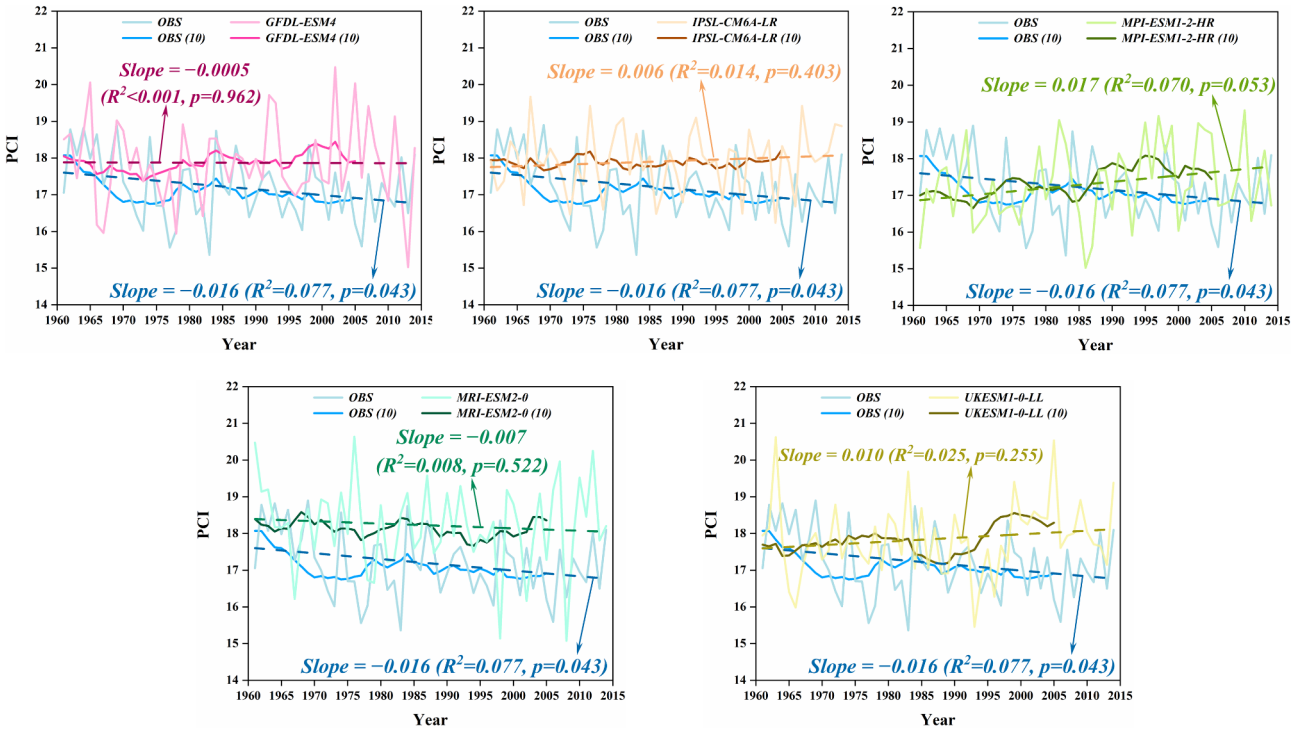

Fig. 4. The same as Fig. 2, but for the PCI.

dynamics within a region. Therefore, it is imperative to conduct a more detailed assessment of the modeling capabilities of each model concerning seasonal precipitation and its variation trends in the SWRB.

An analysis of the spatial distribution of seasonal precipitation derived from both model simulations and observational data in the SWRB (figure not shown) reveals a pattern akin to that observed for annual average precipitation. Notably, all models tend to overestimate seasonal precipitation, with this tendency being particularly pronounced in the Himalayan region. Figure 5 illustrates a Taylor diagram depicting the modeling capacities of the five ISIMIP3b models concerning seasonal precipitation in the SWRB. For spring and summer precipitation, save for the MPI-ESM1-2-HR model, the remaining four models have comparable simulation capabilities. Spatial correlation coefficients fall within the range of 0.60 to 0.80, with ratios of standard deviation between observational and model fields ranging from 1.00 to 1.50, and standardized root-mean-square errors below 1.00. These findings underscore the satisfactory modeling of spring and summer precipitation distribution by these four models in the SWRB. In comparison, modeling capabilities for autumn precipitation exhibit spatially enhanced performance, with spatial correlation coefficients generally ranging from 0.80 to 0.90 for the four models excluding MPI-ESM1-2-HR. Standard deviation ratios of these four models close to 1.00, and standardized root-mean-square errors hover around 0.50, indicating their excellent modeling of autumn precipitation distribution. Conversely, modeling capabilities for winter precipitation are notably constrained for all models, with spatial correlation coefficients ranging from 0.40 to 0.60 and standard deviation ratios surpassing 1.50 for all five models, reaching even beyond 2.00 for the MPI-ESM1-2-HR model. Furthermore, standardized root-mean-square errors exceed 1.00. Hence, it is evident that the ISIMIP3b models excel in simulating the distribution of autumn precipitation in the SWRB, followed by spring and summer, with the poorest performance observed for winter precipitation.

Table S2 provides a comprehensive ranking of the simulation performance of the five ISIMIP3b models regarding seasonal precipitation in the SWRB from 1961 to 2014. For the climatological mean state of spring, summer, and autumn precipitation, the IPSL-CM6A-LR, GFDL-ESM4, and UKESM1-0-LL models demonstrate superior performance. These models exhibit the best spatiotemporal capabilities within their respective seasons. Moreover, these models also rank highly in simulating the climatological mean state of annual average precipitation and annual average PCI. In contrast, the five models' performance in simulating the climatological

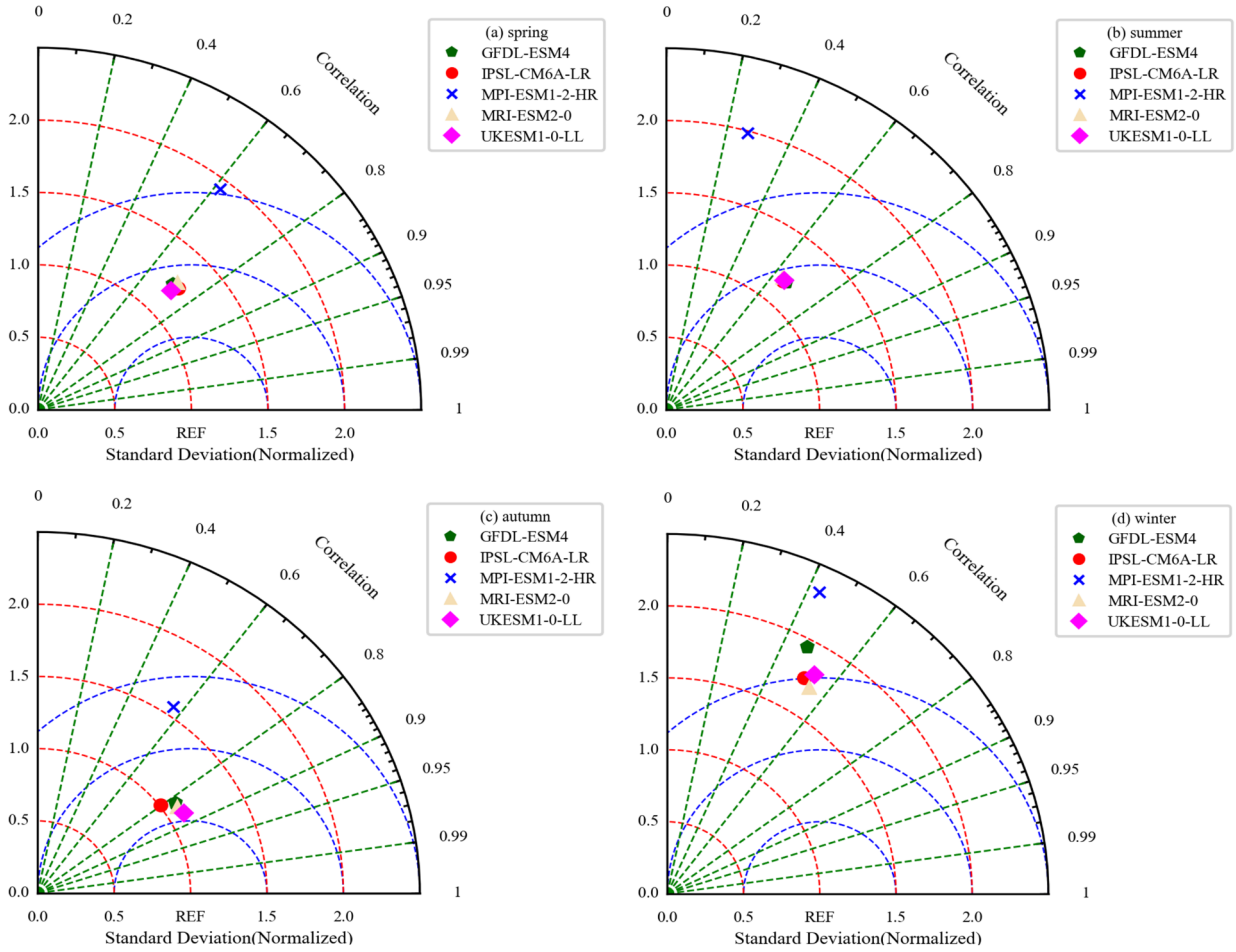

Fig. 5. The Taylor diagram of 5 ISIMIP3b models for the seasonal precipitation in the SWRB from 1961 to 2014.

mean state of winter precipitation is generally moderate, with the IPSL-CM6A-LR, MRI-ESM2-0, and UKESM1-0-LL models showing the best overall performance.

Figure 3 indicates that the PCI values in the SWRB simulated by the five ISIMIP3b models all exhibit varying degrees of overestimation. The seasonal precipitation proportions provide insight into the annual precipitation distribution across different seasons, and can help explain the discrepancies in the models' PCI simulation accuracy. To further investigate, we calculated the spatial grid-based simulation deviations for each model regarding seasonal precipitation proportions in the SWRB and represented the results as boxplots.

As shown in Fig. 6, all models overestimate the spring precipitation proportion in the SWRB. Notably, the median, mean and IQR (Interquartile Range) values of simulation bias in GFDL-ESM4 model reach 0.73%, 1.24% and 3.57%, respectively, which are the maximum values among the five models. Conversely, the MPI-ESM1-2-HR model has the smallest mean and IQR values, at 0.45% and 2.69%, respectively. For the autumn precipitation proportion, the MPI-ESM1-2-HR model performs the best, with the smallest IQR value of 1.61%. The IPSL-CM6A-LR model overestimates this proportion, showing the largest IQR value of 2.32%. The other three models predominantly underestimate the autumn precipitation proportion. Specifically, the MRI-ESM2-0 model has the smallest median (−0.50%), and the UKESM1-0-LL model has the smallest mean (−0.69%), indicating severe underestimation by these two models. Analysis of the boxplots for summer and winter precipitation proportion biases reveals substantial differences between the median and mean values for each model, primarily due to varying degrees of precipitation proportion outliers in the SWRB simulated by ISIMIP3b models. In the meanwhile, there are more negative outliers for summer precipitation proportions and more positive outliers for winter, resulting in the mean values of the boxplots being less than 0 for summer and greater than 0 for winter for all models. Additionally, for the MRI-ESM2-0 model, which shows the largest average PCI simulation bias in Fig. 3, the median values for summer, autumn, and winter precipitation proportions biases are 0.53%, −0.50%, and −0.24%, respectively. This indicates a tendency for the MRI-ESM2-0 model to overestimate summer and underestimate autumn and winter precipitation proportions, leading to a higher simulated PCI.

Given the generally poor simulation performance of the five ISIMIP3b models on the PCI trend variations in the SWRB, we compared their simulation performance on the seasonal precipitation proportion changes to explore the reasons behind this. Table S3 presents the trends in the average seasonal precipitation proportions in

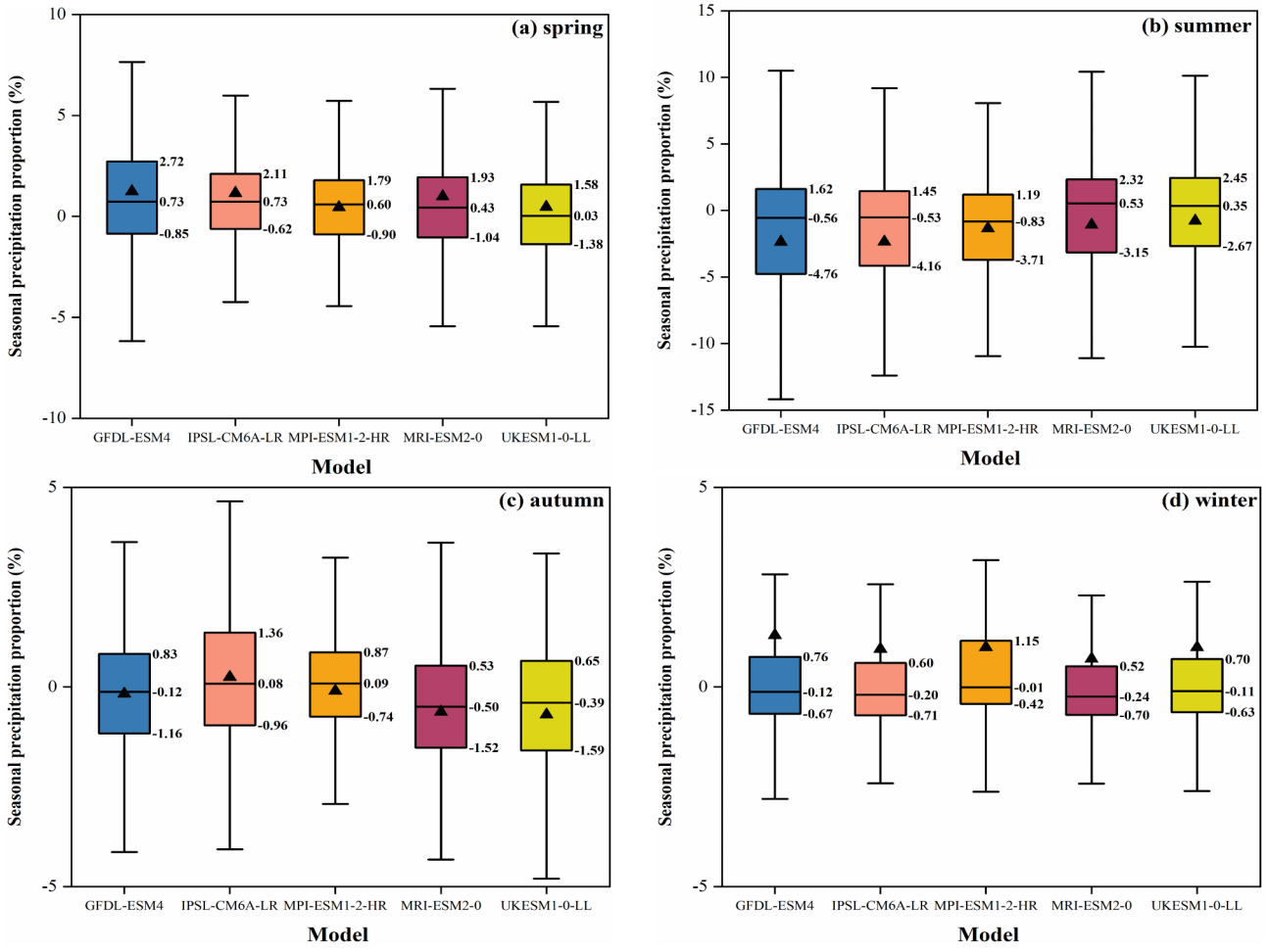

Fig. 6. The boxplots of seasonal precipitation proportion biases in the SWRB from 5 ISIMIP3b models, with "▲" representing the mean of each boxplot.

the SWRB derived from the simulations of the five ISIMIP3b models and the observational data for the period 1961–2014. During this period, the proportion of summer precipitation in the SWRB shows a decreasing trend, with a trend coefficient of −0.79% (10 a)$^{-1}$, passing a 95% significance test. Conversely, the proportions of spring, autumn, and winter precipitation all exhibit increasing trends, with trend coefficients of 0.77% (10 a)$^{-1}$, 0.01% (10 a)$^{-1}$, and 0.01% (10 a)$^{-1}$, respectively, with only the trend coefficient for spring precipitation passing a 99% significance test. Therefore, annual precipitation is distributed more evenly across different seasons, resulting in a decrease in the observed PCI. In addition, only the IPSL-CM6A-LR model performs relatively well in simulating observed trends of seasonal precipitation proportions for spring and summer, capturing the respective increasing and decreasing trends. However, the model does not simulate the statistical significance of these trends, with coefficients of 0.26% (10 a)$^{-1}$ and −0.14% (10 a)$^{-1}$, respectively. For autumn and winter, where observed trends show statistically non-significant increases, all models generally indicate statistically non-significant decreases. Notably, the MPI-ESM1-2-HR model shows a significant decreasing trend in winter precipitation proportions. Overall, the models' representation of seasonal precipitation proportion trends in the SWRB is poor, and thus fails to accurately reflect the long-term trends of PCI.

Discussion

Findings and limitations of the study

This study comprehensively evaluated the simulation performance of 5 GCMs from ISMIP3b regarding characteristics of precipitation changes in the SWRB. The purpose of our study was to provide a basis for model selection in the study of climate change impacts in the SWRB. Previous studies have shown significant differences in the precipitation simulation performance of different models at the regional scale[12]. Therefore, selecting the better models based on the evaluation results could help reduce simulation uncertainty.

In this study, we found that the five ISIMIP3b models generally exhibit a wet bias in simulating precipitation, which is consistent with earlier GCMs. This overestimation can be attributed to several factors, including the complex topography of the SWRB, which current GCMs struggle to accurately capture due to their insufficiently fine resolution, leading to exaggerated orographic precipitation. Additionally, the models' inability to accurately parameterize convective processes, coupled with the overestimation of moisture transport (particularly from monsoonal systems), further contributes to the observed wet bias. The ability of each model to simulate annual and seasonal precipitation in the SWRB is limited. Although all models can generally simulate the distribution pattern of the mean state of precipitation, they consistently overestimate its values in certain areas, especially in the Himalayan region. Moreover, the simulation performance of the five models in capturing trends and interdecadal variations remains limited. These findings are consistent with the research results of Lun et al.[29] and Yang et al.[30].

Our evaluation of PCI and seasonal precipitation proportions revealed that while the models can simulate the intra-annual concentration of precipitation in the SWRB well in terms of space scale, they struggle to accurately characterize the changes in precipitation concentration. This limitation likely arises from several factors, including the models' insufficient spatial resolution, which may fail to reflect localized precipitation patterns and their temporal variability. Furthermore, the models' poor simulation performance for PCI trends is partly due to inadequacies in simulating trends in seasonal precipitation proportions and difficulties in capturing the complex physical and dynamical processes influencing PCI. The variations in PCI are also influenced by the changes in atmospheric circulation[20], and the complex interactions between atmospheric circulation mechanisms and local climate characteristics are difficult to characterize, further contributing to the models' poor representation of PCI trends.

Uncertainty in model results

The uncertainty of climate change simulation and projection are typically attributed to three factors: model uncertainty, internal variability, and scenario uncertainty[31]. Model uncertainty arises from differences in the structure, assumptions, parameterization, and representation of physical processes of different models, which is considered the most influential. Internal variability refers to natural oscillations arising from the dynamic processes within the climate system in the absence of external radiative forcing, such as the Atlantic Multidecadal Oscillation (AMO) and the El Niño-Southern Oscillation (ENSO)[32]. Scenario uncertainty stems from differences in the driving factors of the climate system, including natural forcing factors (such as volcanic eruptions and solar activity) and anthropogenic forcing factors (such as greenhouse gas emissions, aerosol concentrations, and land-use changes). These three factors contribute to deviations between historical simulations and observations, thereby affecting the models' predictive capability and credibility for future climate projections.

Compared to internal variability and scenario uncertainty, model uncertainty can be more effectively reduced through empirical-statistical bias correction methods. However, it is worth mentioning that the selection of bias correction methods and climate forcing datasets used for bias correction of GCMs significantly impacts the reliability of regional climate change predictions, especially for extreme climates[33]. Therefore, it is necessary to further correct ISIMIP3b data based on more accurate observations and reliable bias correction methods to enhance the simulation performance of ISIMIP3b models and reduce uncertainties in future climate projections.

Potential improvements for future research

Firstly, the assessment of precipitation concentration requires further in-depth investigation. The PCI, the most important part of our study, primarily reflects the heterogeneity of monthly precipitation distribution throughout the year and does not address daily scales. To address this, we can use the concentration index (CI) proposed by Martin-Vide[34] to quantify the concentration of daily precipitation, enabling a comprehensive evaluation of the models' performance in simulating both PCI and CI. This would enable a more comprehensive analysis of the

models' representation of precipitation concentration in the SWRB and provide theoretical guidance for climate risk assessment in the region.

Secondly, the ensemble average of multiple models generally performs better than a single model for simulating meteorological elements[35,36]. In this study, while comprehensively evaluating the simulation performance of each ISIMIP3b model for precipitation changes in the SWRB, we also provide the comprehensive rankings under different evaluation targets. If the better models are selected for ensemble averaging, the simulation results obtained should be better than those of a single model. Additionally, our evaluation results also indicate that there is no absolute optimal or worst model. When constructing a model ensemble scheme, assigning different weights to different models according to the precipitation characteristics of interest may improve the simulation performance of the ensemble model.

Furthermore, given the limitations of GCMs in simulating precipitation changes in the SWRB, the most fundamental solution lies in improving the models themselves. One promising approach is the application of machine learning (ML) and artificial intelligence (AI) techniques to enhance the accuracy and reliability of GCMs in climate modeling and prediction[37]. ML and AI technologies offer potential for more accurate climate simulations, typically through three approaches. The first approach involves developing ML models, known as emulators, that produce the same outputs as traditional models and obviate the need for extensive mathematical computations. The second approach leverages AI to uncover previously unknown patterns within vast datasets, these patterns could potentially produce better simulated results than traditional models. The third approach integrates ML components into traditional physics-based models to create hybrid models. This hybrid approach selectively replaces the weaker components of traditional models—often those related to small-scale, complex, and critical processes such as cloud formation, snow cover, and river flows—with AI-driven components, resulting in models that outperform purely physics-based models while maintaining greater trustworthiness than models constructed entirely by AI[38,39]. While ML and AI hold significant promise for improving climate models, their integration into existing modeling frameworks is still in the early stages[40]. Future research should focus on refining these hybrid models to ensure they capture the complexity of climate processes without compromising scientific credibility. As the field progresses, these advanced models may become essential tools in climate impact studies, providing more reliable climate simulations and predictions.

Finally, due to the complex underlying surface conditions in the SWRB, compared to GCMs, regional climate models (RCMs) have a much finer resolution[41,42], allowing the models to use data that are closer to the real terrain for numerical simulation, which may result in better simulation performance for meteorological elements. Therefore, it is essential to compare and analyze the simulation results of GCMs and RCMs.

Conclusions

Based on simulated precipitation data from 5 GCMs in the ISIMIP3b and the observed precipitation dataset CN05.1 spanning 1961–2014, we conducted a comprehensive assessment of these models' performance in simulating precipitation changes in the SWRB. Our evaluation led to the following conclusions:

1) The 5 GCMs can effectively simulate the spatial distribution of annual average precipitation in the SWRB, but they significantly overestimate its magnitude, with a maximum regional average deviation of 207.80 mm (MPI-ESM1-2-HR). Overall, the IPSL-CM6A-LR model performs best in simulating the annual precipitation on both spatial and temporal scales, achieving the highest comprehensive ranking. All GCMs struggle to accurately depict the spatial distribution of trends in annual average precipitation in the SWRB, often overestimating the overall aridity. Among these models, the MPI-ESM1-2-HR model shows relatively better performance with a TS value of 0.676. Significant differences exist in the simulation performance of the five GCMs regarding the interdecadal variations in precipitation in the SWRB.
2) The 5 GCMs exhibit good performance in simulating the spatial distribution of annual average PCI in the SWRB, although they generally overestimate its values, with a maximum regional average deviation of 1.54 (MRI-ESM2-0). Overall, the MPI-ESM1-2-HR model performs best in simulating the annual average PCI, with the highest TS value and the lowest IVS value. All models show limited capability in simulating the spatial distribution of trends in the annual average PCI in the SWRB, with only the UKESM1-0-LL model demonstrating relatively better performance, achieving a TS value of 0.771. The simulation performance of all models is generally poor regarding the interdecadal variations in PCI in the SWRB.
3) The 5 GCMs consistently overestimate the precipitation values across all seasons in the SWRB. All models perform best in simulating autumn precipitation distribution, followed by spring and summer, with the poorest performance in winter. The boxplots of seasonal precipitation proportion biases reveal significant differences in the simulation results, with the MRI-ESM2-0 model tending to overestimate summer precipitation proportions and underestimate those of autumn and winter, resulting in the largest average simulation deviation of the PCI. Furthermore, all models exhibit poor performance in simulating the trends of seasonal precipitation proportions in the SWRB, consequently failing to accurately reflect the long-term PCI trends.

Data availability

This study used historical daily gridded precipitation data of five ISIMIP3b models from the ISIMIP3b bias-adjusted atmospheric climate input data (v1.1). These ISIMIP3b datasets are available on the ISIMIP official website (https://www.isimip.org/, DOI: https://doi.org/10.48364/ISIMIP.842396.1). The gridded observational precipitation dataset (CN05.1) can be obtained from the Climate Research Open Laboratory of the China Meteorological Administration and is accessible at https://ccrc.iap.ac.cn/resource. The datasets used and analyzed during this study are available from the corresponding author upon reasonable request.

Received: 30 May 2024; Accepted: 20 September 2024
Published online: 28 September 2024

References

1. Trenberth, K. Changes in precipitation with climate change. *Clim. Res.* **47**, 123–138 (2011).
2. Rhodes, C. J. Only 12 years left to readjust for the 1.5-degree climate change option—Says International Panel on Climate Change report: Current commentary. *Sci. Prog.* **102**, 73–87 (2019).
3. Matthews, H. D. & Wynes, S. Current global efforts are insufficient to limit warming to 1.5 °C. *Science*. **376**, 1404–1409 (2022).
4. Li, L. et al. Trends, change points and spatial variability in extreme precipitation events from 1961 to 2017 in China. *Hydrol. Res.* **51**, 484–504 (2020).
5. Qu, B., Lv, A., Jia, S. & Zhu, W. Daily precipitation changes over large river basins in China, 1960–2013. *Water*. **8**, 185 (2016).
6. Li, Y., Yan, D., Peng, H. & Xiao, S. Evaluation of precipitation in CMIP6 over the Yangtze River Basin. *Atmos. Res.* **253**, 105406 (2021).
7. Pan, H., Jin, Y. & Zhu, X. Comparison of projections of precipitation over Yangtze River Basin of China by different climate models. *Water*. **14**, 1888 (2022).
8. Meehl, G. A. et al. Climate Model intercomparisons: Preparing for the next phase. *EoS Trans.* **95**, 77–78 (2014).
9. Rosenzweig, C. et al. Assessing inter-sectoral climate change risks: The role of ISIMIP. *Environ. Res. Lett.* **12**, 010301 (2017).
10. Hempel, S., Frieler, K., Warszawski, L., Schewe, J. & Piontek, F. A trend-preserving bias correction—The ISI-MIP approach. *Earth Syst. Dynam*. **4**, 219–236 (2013).
11. Salaudeen, A., Ismail, A., Adeogun, B. K., Ajibike, M. A. & Shahid, S. Assessing the skills of inter-sectoral impact model intercomparison project climate models for precipitation simulation in the Gongola Basin of Nigeria. *Sci. Afr.* **13**, e00921 (2021).
12. Hawkins, E. & Sutton, R. The potential to narrow uncertainty in projections of regional precipitation change. *Clim. Dyn.* **37**, 407–418 (2011).
13. Kamworapan, S. & Surussavadee, C. Evaluation of CMIP5 global climate models for simulating climatological temperature and precipitation for Southeast Asia. *Adv. Meteorol*. 1–18 (2019).
14. Zhou, T. et al. Development of Climate and Earth System models in China: Past achievements and new CMIP6 results. *J. Meteorol. Res.* **34**, (2020).
15. Jia, K., Ruan, Y., Yang, Y. & Zhang, C. Assessing the performance of CMIP5 global climate models for simulating future precipitation change in the Tibetan Plateau. *Water*. **11**, 1771 (2019).
16. Fiedler, S. et al. Simulated tropical precipitation assessed across three major phases of the coupled model Intercomparison Project (CMIP). *Mon. Weather Rev.* **148**, 3653–3680 (2020).
17. Bartolini, G., Grifoni, D., Magno, R., Torrigiani, T. & Gozzini, B. Changes in temporal distribution of precipitation in a Mediterranean area (Tuscany, Italy) 1955–2013. *Intl J. Climatol.* **38**, 1366–1374 (2018).
18. Tolika, K. On the analysis of the temporal precipitation distribution over Greece using the Precipitation Concentration Index (PCI): annual, seasonal, monthly analysis and association with the atmospheric circulation. *Theor. Appl. Climatol.* **137**, 2303–2319 (2019).
19. Oliver, J. E. & Monthly precipitation distribution a comparative index. *Prof. Geogr.* **32**, 300–309 (1980).
20. De Luis, M., González-Hidalgo, J. C., Brunetti, M. & Longares, L. A. Precipitation concentration changes in Spain 1946–2005. *Nat. Hazards Earth Syst. Sci.* **11**, 1259–1265 (2011).
21. Lu et al. Spatial and temporal variability in Precipitation Concentration over Mainland China, 1961–2017. *Water*. **11**, 881 (2019).
22. Tehreem, Z. et al. A Novel Appraisal Protocol for Spatiotemporal patterns of rainfall by reconnaissance the Precipitation Concentration Index (PCI) with global warming context. *Math. Probl. Eng.* **2022**, 1–9 (2022).
23. Du, J., Yu, X., Zhou, L., Li, X. & Ao, T. Less concentrated precipitation and more extreme events over the Three River Headwaters region of the Tibetan Plateau in a warming climate. *Atmos. Res.* **303**, 107311 (2024).
24. Wu, J. & Gao, X. J. A gridded daily observation dataset over China region and comparison with the other datasets. *Chin. J. Geophys. (in Chinese)*. **56**, 1102–1111 (2013).
25. Jägermeyr, J. et al. Climate impacts on global agriculture emerge earlier in new generation of climate and crop models. *Nat. Food*. **2**, 873–885 (2021).
26. Taylor, K. E. Summarizing multiple aspects of model performance in a single diagram. *J. Geophys. Res.* **106**, 7183–7192 (2001).
27. Chen, W., Jiang, Z. & Li, L. Probabilistic projections of Climate Change over China under the SRES A1B scenario using 28 AOGCMs. *J. Clim.* **24**, 4741–4756 (2011).
28. Tang, B., Hu, W. & Duan, A. Future projection of Extreme Precipitation indices over the Indochina Peninsula and South China in CMIP6 models. *J. Clim.* **34**, 8793–8811 (2021).
29. Lun, Y. et al. Assessment of GCMs simulation performance for precipitation and temperature from CMIP5 to CMIP6 over the Tibetan Plateau. *Int. J. Climatol.* **41**, 3994–4018 (2021).
30. Yang, X., Zhou, B., Xu, Y. & Han, Z. CMIP6 evaluation and projection of temperature and precipitation over China. *Adv. Atmos. Sci.* **38**, 817–830 (2021).
31. Cox, P. & Stephenson, D. A changing climate for prediction. *Science*. **317**, 207–208 (2007).
32. Prigent, A., Imbol Koungue, R. A., Nkwinkwa, I., Beobide-Arsuaga, A. S. N. & Farneti, R. G. Uncertainty on Atlantic Niño variability projections. *Geophys. Res. Lett.* **50**, eGL105000 (2023).
33. Iizumi, T., Takikawa, H., Hirabayashi, Y., Hanasaki, N. & Nishimori, M. Contributions of different bias-correction methods and reference meteorological forcing data sets to uncertainty in projected temperature and precipitation extremes. *JGR Atmos.* **122**, 7800–7819 (2017).
34. Martin-Vide, J. Spatial distribution of a daily precipitation concentration index in peninsular Spain. *Intl J. Climatol.* **24**, 959–971 (2004).
35. Pierce, D. W., Barnett, T. P., Santer, B. D. & Gleckler, P. J. Selecting global climate models for regional climate change studies. *Proc. Natl. Acad. Sci. U.S.A.* 106, 8441–8446 (2009).
36. Slater, L. J., Villarini, G. & Bradley, A. A. Evaluation of the skill of North-American Multi-model Ensemble (NMME) Global Climate models in predicting average and extreme precipitation and temperature over the continental USA. *Clim. Dyn.* **53**, 7381–7396 (2019).
37. Watt-Meyer, O. et al. Correcting weather and climate models by machine learning nudged historical simulations. *Geophys. Res. Lett.* **48**, e2021GL092555 (2021).
38. Jones, N. How machine learning could help to improve climate forecasts. *Nature*. **548**, 379–379 (2017).
39. Wong, C. How AI is improving climate forecasts. *Nature* **628**, 710–712 (2024).
40. de Burgh-Day, C. O. & Leeuwenburg, T. Machine learning for numerical weather and climate modelling: A review. *Geosci. Model Dev.* **16**, 6433–6477 (2023).
41. Beniston, M. et al. Future extreme events in European climate: An exploration of regional climate model projections. *Clim. Change*. **81**, 71–95 (2007).
42. Semenov, M. & Stratonovitch, P. Use of multi-model ensembles from global climate models for assessment of climate change impacts. *Clim. Res.* **41**, 1–14 (2010).

Acknowledgements
We gratefully acknowledge the Key R&D Project from the Science and Technology Department of Tibet (XZ202101ZY0007G). We also thank the Inter-Sectoral Impact Model Intercomparison Project (ISIMIP) and the China Meteorological Administration (CMA) for making the relevant data publicly available.

Author contributions
Y.K.Z. conceived the idea, worked, analyzed, and wrote the manuscript. J.D. developed the idea, and helped in writing and visualizing. Y.B.D. and L.L.W. helped in interpreting the results. T.Q.A. was responsible for supervision and provided support. All authors reviewed the manuscript.

Declarations

Competing interests
The authors declare no competing interests.

Additional information
Supplementary Information The online version contains supplementary material available at https://doi.org/10.1038/s41598-024-73741-w.

Correspondence and requests for materials should be addressed to J.D. or T.A.